Frontiers of Information Technology & Electronic Engineering
www.jzus.zju.edu.cn; engineering.cae.cn; www.springerlink.com
ISSN 2095-9184 (print); ISSN 2095-9230 (online)
E-mail: jzus@zju.edu.cn

Frequency of arrival-based state estimation and trajectory optimization for the navigation of autonomous marine vehicles#

Sitian WANG[1], Huarong ZHENG[†‡2], Jianlong LI[1], Wen XU[2,3]

[1]*College of Information Science and Electronic Engineering, Zhejiang University, Hangzhou 310027, China*

[2]*Ocean college, Zhejiang University, Zhoushan 316021, China*

[3]*Institute of Deep-sea Science and Engineering, Chinese Academy of Sciences, Sanya 572000, China*

[†]E-mail: hrzheng@zju.edu.cn

Received Apr. 12, 2025; Revision accepted Aug. 25, 2025; Crosschecked Sept. 17, 2025

Unedited

Abstract: Using global positioning system (GPS) and the mobility of marine surface vehicles, this paper addresses the navigation problem between unmanned surface vehicles (USVs) and autonomous underwater vehicles (AUVs). We propose a moving AUV state estimation method based on the trajectory optimization of the USV. In particular, by exploring the Doppler effect on the frequency of arrival (FOA) of the acoustic signals received by a single-surface USV, the position and velocity of the AUV can be estimated simultaneously, offering a robust solution that eliminates the need for time synchronization. Moreover, the USV trajectory is dynamically adjusted to achieve optimal USV–AUV measurement geometry, thereby improving AUV observability and enhancing state estimation performance. The innovation lies in a tailored cost function grounded in observability analysis via the Cramér-Rao lower bound (CRLB) and geometric constraints. It integrates (1) the CRLB to optimize system observability, thereby enhancing estimation accuracy, (2) a distance term that ensures the USV maintains appropriate proximity to the AUV, and (3) a turning rate term that adjusts the USV's orientation to improve following capability. The cost function is then minimized using a particle swarm optimization algorithm, balancing these components to achieve a robust AUV tracking framework. We conduct comprehensive simulations to examine the potential influences of different factors, including the complexity of the USV trajectory, AUV depth, measurement frequency, packet loss rate, and noise levels, on navigation performance. Simulation results demonstrate the effectiveness of the proposed method in estimating and tracking the AUV.

Key words: Frequency of arrival; Rolling horizon estimation; Trajectory optimization; Unmanned surface vehicles; Autonomous underwater vehicles; Navigation

https://doi.org/10.1631/FITEE.2500235 **CLC number:**

1 Introduction

Scientific research and technological applications are being actively conducted worldwide to better understand the ocean. Regardless of the specific application, the precise state estimation of underwater platforms, such as autonomous underwater vehicles (AUVs), is fundamental and crucial (Zhang BB et al., 2023; Yu et al., 2025). Various state estimation systems have been developed using acoustic signals, as radio waves are significantly attenuated in water. Due to the absence of a global positioning system (GPS) underwater, acoustic baseline-based

‡ Corresponding author

Electronic supplementary materials: The online version of this article (https://doi.org/10.1631/FITEE.2500235) contains supplementary materials, which are available to authorized users

ORCID: Sitian WANG, https://orcid.org/0000-0002-3628-0126

© Zhejiang University Press 2025

techniques have been widely used for AUV position estimation.

Acoustic baseline-based underwater positioning systems have exhibited satisfactory performance under certain circumstances, including the long baseline (LBL) (Lee and Jun, 2007), ultra short baseline (USBL) (Guo et al., 2023), and GPS intelligent buoys (GIB) (Zhang DQ et al., 2020), among others. Most of these baseline localization systems are based on measuring the time of arrival (TOA) of the acoustic signals. Furthermore, different baseline localization techniques can be combined whenever necessary.

The frequency of arrival (FOA)-based state estimation methods, which can be considered a type of angle of arrival (AOA) methods (Win et al., 2008; Gong et al., 2023; Xu et al., 2023), have not received as much attention as the aforementioned traditional TOA-based methods due to their modeling and analysis complexity. Nonetheless, the benefit of FOA-based methods is that they can estimate a target's position and velocity simultaneously without requiring time synchronization (Cameron, 2018; Zhan et al., 2023). Kim (2023) proposed a hybrid time difference of arrival (TDOA) and frequency difference of arrival (FDOA) localization method for underwater targets. This method contains multiple frequencies in the transmitted acoustic signal, and the localization performance is satisfactory. Multiple acoustic sensor nodes are typically installed on the seabed or float on the sea surface in the previously mentioned acoustic baseline-based or FOA-based approaches. The AUV's operational region is constrained by its narrow visible range.

Single-node localization techniques have been suggested to simplify the system and make deployment easier (Webster et al., 2012; Han et al., 2018). With only a single sensor node, the AUV must be located using the node's historical measurement data collected along a given trajectory. Single-node underwater acoustic localization methods can be roughly categorized into two categories based on different localization principles. The first category relies on the measured target states, such as bearing measurements (Becker et al., 2012), frequency measurements (Nguyen and Dogancay, 2018), distance measurements (Zhu and Hu, 2018), or a combination of the aforementioned measurements. The target position can then be determined using triangulation equations. Note that the FOA method with a single moving sensor is suggested in (Nguyen and Dogancay, 2018). Since the target (or sensor) is moving, the Doppler effect can be used to estimate the target's velocity.

The second category of methods is based on filtering techniques for tracking and localization of underwater targets (De Palma et al., 2017). THese methods leverage the current and historical target states to minimize estimation variances. The extended Kalman filter (EKF) can be used when planning a surface vehicle's path to accomplish range-only AUV localization. Researchers at the Massachusetts Institute of Technology (MIT) have given careful consideration to such navigation problems, which include the single sensor node problems mentioned above (Tan et al., 2014; Rypkema, 2019). A surface vessel can be deployed for navigation when the AUV is equipped with inexpensive localization sensors. To locate the AUV, one-way travel times between the AUV and the surface sensor node are measured in Fallon et al. (2010). A comparison of the localization performance for the EKF, particle filter, and nonlinear least squares estimator reveals that the nonlinear least squares estimator demonstrates the best performance.

However, the observability issue deserves particular attention in the single-node localization problem. To extract the target state information from measurements, the localization system must be observable (Ostachowicz et al., 2019). Localization performance is strongly influenced by the geometric relationship between the sensor and the target. Different geometric configurations—resulting from the sensor node moving with the surface vehicle in different trajectories—correspond to different target observability and, thus to different localization performance. The target observability can be analytically characterized by the Fisher information matrix (FIM) (Chen et al., 2015; Qu et al., 2021) or the Cramér-Rao lower bound (CRLB) (Moreno-Salinas et al., 2016). Properties of the FIM and CRLB matrices, such as determinant, trace, or eigenvalues, can serve as indices of the target observability (Conti et al., 2019; Sahu et al., 2022). This target observability information can be used to enhance the system observability by optimizing the sensor node trajectory.

In this paper, we extend the navigation con-

Unedited

cept by estimating the AUV states using a single surface sensor node on an unmanned surface vehicle (USV) (Zheng and Liu, 2025). Since the AUV and USV are both moving, the AUV's position and velocity can be determined by analyzing the Doppler effect in the FOA. The estimation task is completed by combining historical FOA measurements along the USV trajectory. The USV trajectory is dynamically changed to attain an ideal measurement geometry, thereby further enhancing the estimation performance. The estimation performance is represented by the degree of system observability, which is modeled by the FOA-dependent FIM. We generate the USV trajectory that optimizes the AUV state estimation performance by minimizing the CRLB. In essence, the mobility of the USV and the GPS on the surface enable estimation and additional performance enhancement. Therefore, we refer to the issue as USV–AUV navigation.Furthermore, we investigate the influence of various factors on the estimation performance is also investigated using the suggested formulations of the FOA-based state estimation problem. The guidelines for applying FOA-based estimation techniques could be found in these investigations.

Overall, this work contributes to the literature on the following three aspects:

1. A novel FOA-based navigation framework for simultaneously estimating the position and velocity states of AUVs is proposed for scenarios where only a single surface sensor node exists.

2. Estimation performance indices are proposed and optimized for the FOA-based estimation techniques by leveraging the mobility of the USV.

3. Comprehensive results and analysis are provided to the field with guidelines on using FOA-based estimation techniques.

2 Problem statement and modeling

Considering the AUV as the underwater target and the USV as the surface sensor node, we apply the navigation concept to the problem under consideration. The state estimation problem based on the USV–AUV FOA is then formally introduced. Additionally, the USV kinematic model and the FOA measurement model are presented for subsequent FOA-based state estimation and performance optimization.

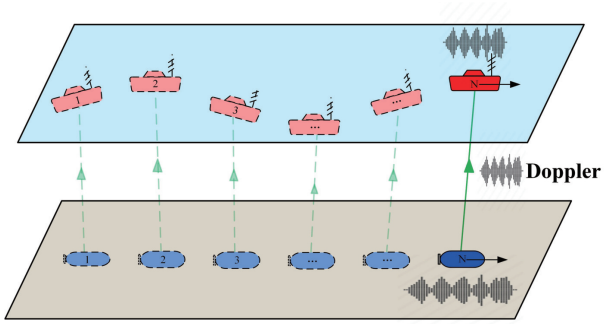

Fig. 1 Illustration of the FOA-based state estimation problem for USV–AUV. A USV (red vehicle) moves at the water surface, while an AUV (blue vehicle) moves underwater at a slowly varying speed. The green line represents the propagation path of the acoustic signals emitted by the AUV and received by the USV. The light-colored vehicles with dashed lines represent the historical states, whereas the darkcolored vehicles with solid lines represent the current states. References to color refer to the online version of this figure

2.1 Problem statement

We consider the situation illustrated in Fig. 1, where an AUV periodically transmits acoustic signals to a USV while moving underwater at a slowly changing velocity. The FOA measurement is extracted by filtering the acoustic signals after the USV receives them. Traditionally, to solve the state estimation problem, multiple sensor nodes are usually required to obtain various measurements. In contrast, when using a single USV, various historical measurements from the USV are investigated, mimicking the situation with multiple nodes.

The USV can estimate the current AUV state by using N historical FOA measurements. As the surface-moving sensor node, the USV trajectory significantly affects the accuracy of AUV state estimation. By optimizing the USV trajectory with certain constraints, AUV observability, and consequently, the accuracy of the state estimation can be improved.

Therefore, the USV–AUV FOA-based state estimation problem is characterized by the following features:

1. A single sensor node instead of multiple sensor nodes is deployed, which reduces costs.

2. The mobility of the USV enables a larger operational range for the AUV.

3. The mobility of the USV offers the degree of freedom to dynamically optimize the measurement geometry, and thus improve the estimation perfor-

Unedited

mance.

4. The dynamic motions of the USV and AUV offer the possibility of simultaneous position and velocity estimation by exploring the Doppler effect.

2.2 USV and AUV kinematic modeling

The USV moves in a horizontal plane over the sea surface (Zheng et al., 2024). The state of the USV at the ith measurement step is described as follows:

$$\boldsymbol{x}_{\text{s}}(i) = [x_{\text{s}}(i), y_{\text{s}}(i), z_{\text{s}}(i), \psi_{\text{s}}(i)]^{\text{T}}, \tag{1}$$

where the subscript $\cdot_{\text{s}}$ is used for the USV state to differ from the AUV state. The discrete time index i relates to the continuous time t vis $t = iT_0$, where T_0 is the sampling interval between consecutive measurement steps. $[x_{\text{s}}(i), y_{\text{s}}(i)]^{\text{T}}$ is the horizontal position of USV on the surface. $\psi_{\text{s}}(i)$ is the heading angle, and the depth $z_{\text{s}}(i)$ denotes the USV's vertical position. We assume the depth is not actively controlled by the USV, but rather fluctuates primarily due to the influence of wave.

For the control of the USV, the input vector at the measurement step i is denoted as $\boldsymbol{u}_{\text{s}}(i) = [v_{\text{s}}(i), \omega_{\text{s}}(i)]^{\text{T}}$, where $v_{\text{s}}(i)$ and $\omega_{\text{s}}(i)$ represent the USV's speed and turning rate in the horizontal plane, respectively. It is assumed, within a measurement step, that the USV moves along a straight line at a constant speed. Therefore, the discrete-time kinematic model of the USV can be expressed as follows:

$$\boldsymbol{x}_{\text{s}}(i+1) = \boldsymbol{x}_{\text{s}}(i) + \begin{bmatrix} v_{\text{s}}(i)\cos\psi_{\text{s}}(i) \\ v_{\text{s}}(i)\sin\psi_{\text{s}}(i) \\ 0 \\ \omega_{\text{s}}(i) \end{bmatrix} T_0 + \boldsymbol{w}_s, \tag{2}$$

where the USV state noise is denoted as $\boldsymbol{w}_s \sim N(0, \boldsymbol{Q}_s)$, with

$$\boldsymbol{Q}_s = \begin{bmatrix} \frac{1}{4}{T_0}^4\boldsymbol{I}_3 & \frac{1}{2}{T_0}^3\boldsymbol{1}_{3\times1} \\ \frac{1}{2}{T_0}^3\boldsymbol{1}_{1\times3} & {T_0}^2 \end{bmatrix}\sigma^2_{\text{s,a}}, \tag{3}$$

where $\boldsymbol{I}_3$ represents the third-order identity matrix and $\boldsymbol{1}_{1\times3}$ represents the 1×3 matrix of ones. $\sigma^2_{\text{s,a}}$ denotes the variance of the Gaussian white noise associated with the USV's acceleration. This paper models the noise as Gaussian, which is a valid and appropriate assumption for stable marine environments (Fossen, 2011; Wang et al., 2025).

Similarly, we define the AUV state vector at the ith measurement step as $\boldsymbol{x}_{\text{u}}(i) = \left[\boldsymbol{p}_{\text{u}}^{\text{T}}(i), \boldsymbol{v}_{\text{u}}^{\text{T}}(i)\right]^{\text{T}}$, where $\boldsymbol{p}_{\text{u}}(i) = [x_{\text{u}}(i), y_{\text{u}}(i), z_{\text{u}}(i)]^{\text{T}}$ and $\boldsymbol{v}_{\text{u}}(i) = [v_{\text{u},x}(i), v_{\text{u},y}(i), v_{\text{u},z}(i)]^{\text{T}}$ represent the three-dimensional position and velocity vectors, respectively. The subscript $\cdot_{\text{u}}$ denotes the AUV state.

Assuming that the AUV accelerations in three directions are subject to independently distributed Gaussian white noise with a common variance of $\sigma^2_{\text{u,a}}$. With the slowly varying velocity assumption, the discrete-time AUV state equation can be expressed as

$$\boldsymbol{x}_{\text{u}}(i+1) = \boldsymbol{F}\boldsymbol{x}_{\text{u}}(i) + \boldsymbol{w}_{\text{u}}, \tag{4}$$

where

$$\boldsymbol{F} = \begin{bmatrix} \boldsymbol{I}_3 & T_0\boldsymbol{I}_3 \\ \boldsymbol{0}_3 & \boldsymbol{I}_3 \end{bmatrix}, \tag{5}$$

where $\boldsymbol{0}_3$ represents the third-order zero matrix. The AUV state noise is $\boldsymbol{w}_{\text{u}} \sim N(0, \boldsymbol{Q}_{\text{u}})$, with

$$\boldsymbol{Q}_{\text{u}} = \begin{bmatrix} \frac{1}{4}{T_0}^4\boldsymbol{I}_3 & \frac{1}{2}{T_0}^3\boldsymbol{I}_3 \\ \frac{1}{2}{T_0}^3\boldsymbol{I}_3 & {T_0}^2\boldsymbol{I}_3 \end{bmatrix}\sigma^2_{\text{u,a}}. \tag{6}$$

2.3 Measurement model

The FOA measurement model is essential to the estimation problem. At each measurement step, the USV measures a noisy FOA f from the acoustic signal transmitted by the AUV. Influenced by the Doppler effect, each FOA measurement provides an equation relating the AUV's position and velocity. Multiple FOA measurements can be used to form a system of nonlinear equations. This system is solvable for the unknown position and velocity when the measurements are linearly independent, as validated in Wang et al. (2025). To estimate the current AUV state (position and velocity), N historical FOA measurements are required (Since the AUV states is defined by six variables, $N \geq 6$), i.e.,

$$\boldsymbol{f}(i) = [f(i-N+1), f(i-N+2), ..., f(i)]^{\text{T}}. \tag{7}$$

The measured noisy FOA $f(i)$ is defined by

$$f(i) = g(i) + \xi(i), \tag{8}$$

where $g(i)$ is the FOA that relates to the USV and AUV states as

$$g(i) = f_0\frac{c_0 - v_{\text{s},\perp}(i)}{c_0 - v_{\text{u},\perp}(i)}, \tag{9}$$

where f_0 is the carrier frequency, c_0 is the speed of sound, and $v_{\text{u},\perp}(i)$ and $v_{\text{s},\perp}(i)$ represent the radial

Unedited

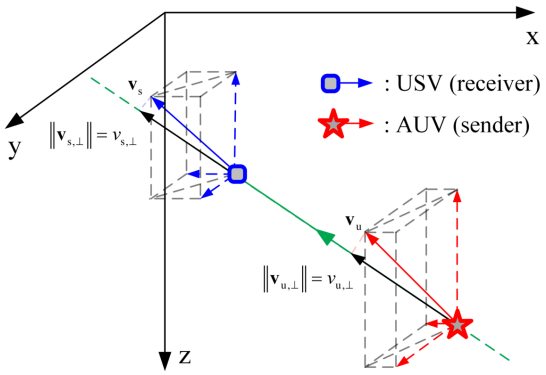

Fig. 2 Decomposition of velocities. The pentagram represents the AUV which sends the acoustic signal with a radial velocity of $v_{\mathrm{u},\perp}$ in the direction of signal propagation. The box represents the USV that receives the signal, and the radial velocity in the direction of signal propagation is $v_{\mathrm{s},\perp}$

velocities of the signal sending (AUV) and receiving (USV) nodes, respectively. As illustrated in Fig. 2, $v_{\mathrm{u},\perp}(i)$ and $v_{\mathrm{s},\perp}(i)$ are measured along the directions of signal propagation.

Note that the AUV depth can be easily measured using a pressure sensor, with Gaussian noise $\xi \sim \mathcal{N}\left(0, \sigma_z^2\right)$. The sound speed is also subject to Gaussian noise $\xi_c \sim \mathcal{N}\left(0, \sigma_c^2\right)$. Communication occurs between the AUV and the USV, where the AUV sends its depth to the USV. Assume a packet loss rate of P_l. If the AUV depth information for the current measurement step is lost, the most recent available depth is used instead.

In Eq. (8), the parameter $\xi(i)$ represents the stochastic Gaussian measurement noise, and $\xi(i) \sim \mathcal{N}\left(0, \sigma^2(i)\right)$. The covariance matrix of the noise vector over the past N steps is then

$$\boldsymbol{R}_\xi(i) = \begin{bmatrix} \sigma^2(i)\boldsymbol{I}_N & \boldsymbol{0}_{N\times 1} \\ \boldsymbol{0}_{1\times N} & \sigma_z^2 \end{bmatrix}, \tag{10}$$

$$\sigma^2(i) = K_{\mathrm{E}} A\left(l(i), f_0\right), \tag{11}$$

where $\sigma^2(i)$ is the distance-dependent noise, K_{E} is a constant related to the transmit power and environment noise level, and $A\left(l(i), f_0\right)$ denotes the pass loss at frequency f_0, which is defined as (Stojanovic and Preisig, 2009)

$$A\left(l(i), f_0\right) = \left(\frac{l(i)}{l_0}\right)^{\beta} L(f_0)^{l(i)-l_0}, \tag{12}$$

where $l(i) = \|\boldsymbol{x}_{\mathrm{u}}(i) - \boldsymbol{x}_{\mathrm{s}}(i)\|$ is the propagation distance, l_0 is the reference distance, and β denotes the path loss exponent, which is commonly 1–2. An empirical formula for the absorption coefficient $L(f_0)$ can be found in Kinsler et al. (2000). The corresponding parameters used are as follows: $l_0 = 1$ m, $\beta = 2$, $K_E = -100$ dB, and $L(f_0) < 3$ dB/km when the frequency is <20 kHz, as illustrated in Fig. 1 in Stojanovic and Preisig (2009). Table 1 lists the typical values of $\sigma^2(i)$ with varying distances and frequencies.

Table 1 Measurement noise $\sigma^2(i)$ (Hz^2 in dB)

$l(i)$ (m)	$\sigma^2(i)$ (Hz^2 in dB)			
	5000 Hz	10 000 Hz	15 000 Hz	20 000 Hz
70	−63.07	−63.02	−62.94	−62.84
100	−59.97	−59.89	−59.78	−59.63
130	−57.68	−57.58	−57.43	−57.24

Unedited

3 FOA-based rolling horizon AUV state estimation and solution

This section focuses on estimating the state of a moving AUV using only a single USV. Typically, multiple measurements are required to solve the state estimation problem. When using a single USV, we combine multiple measurements from the past time steps.

Briefly, with the known historical noisy FOA $f(i)$ measurements, we can estimate the FOA $g(i)$ information, which is related to the AUV and USV states as shown in Eq. (9). Since the historical USV states are available at the surface via GPS, and the historical AUV states are relate to the current AUV states as described in Eq. (4), the current AUV state can be estimated using the EKF (Jiang et al., 2021).

For $k = 0, ..., N-1$,

$$\boldsymbol{x}_{\mathrm{u}}(i-k-1|i) = \begin{bmatrix} \boldsymbol{I}_3 & -T_0\boldsymbol{I}_3 \\ \boldsymbol{0}_3 & \boldsymbol{I}_3 \end{bmatrix} \boldsymbol{x}_{\mathrm{u}}(i-k|i), \tag{13}$$

$$g(i-k|i) = f_0 \frac{c_0 - v_{\mathrm{s},\perp}(i-k|i)}{c_0 - v_{\mathrm{u},\perp}(i-k|i)}, \tag{14}$$

$$r(i-k|i) = f(i-k|i) - g(i-k|i), \tag{15}$$

where the notation $(i-k|i)$ indicates the kth historical step starting backwards from the current step i, $\boldsymbol{x}_{\mathrm{u}}(i|i) = \boldsymbol{x}_{\mathrm{u}}(i)$, and $\boldsymbol{r}(i) = [r(i-N+1|i), ..., r(i|i), 0]^{\mathrm{T}}$. The sequential EKF

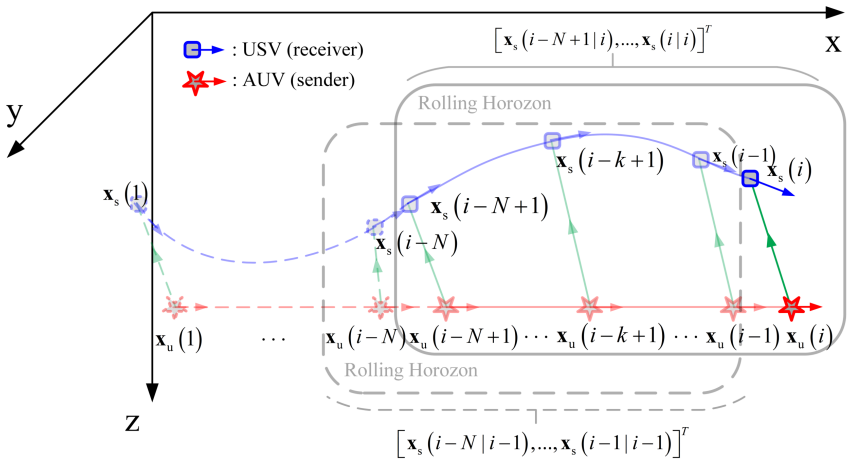

Fig. 3 For each step i, the historical N FOA measurements $g(i-k|i)$ and USV state measurements $\boldsymbol{x}_{\mathrm{s}}(i-k|i)$ for $k=0,\ldots,N-1$ are used to estimate the current AUV state. At step $i+1$, the set of historical measurements is shifted one step forward, and the estimation process is repeated, accounting for the rolling horizon estimation

can be used to solve the above problem iteratively. The recursive solution process is detailed in section 1 of the supplementary materials.

The dynamic AUV state is estimated as the new USV state, and FOA measurements become available. In particular, the most recent N measurements $(i+1-k|i+1)$ for $k=0,\ldots,N-1$ are combined at the next step $(i+1)$ to formulate the estimation problem defined in Eqs. (13)–(15). Then the new AUV state can be estimated with the new measurements. This enables the continuous AUV state estimation in a rolling horizon way, as illustrated in Fig. 3.

4 Trajectory optimization of the USV to maximize the observability

The AUV state is continuously estimated using the USV's measurements. The AUV then obtains its estimated state from the USV. Since the measuring geometry has a significant influence on the estimation performance, this section considers optimizing the USV trajectory to maximize the system observability. We propose using the CRLB that depends on the USV trajectories and the AUV estimated states as the observability index. By minimizing the CRLB, the optimal USV trajectory and, consequently, the optimal FOA measurement geometry can be obtained. To solve the trajectory optimization problem efficiently, a particle swarm optimization (PSO) algorithm is applied.

4.1 Observability performance index

When estimating the state of an AUV, it is crucial to ensure that the AUV possesses adequate observability. FIM measures the amount of information about the AUV state contained in the observation data, thus serving as an effective observability index in estimation problems. The derivations of FIM are presented in section 2 of the supplementary materials.

The CRLB represents the minimum achievable estimation error. It can be obtained by taking the diagonal elements of the inverse of the FIM:

$$\boldsymbol{b}(i)=\mathrm{diag}\left(\boldsymbol{J}(i)^{-1}\right). \tag{16}$$

We use the CRLB as the cost function to maximize the observability. The optimal USV state over a future horizon can be uncovered by optimizing $\boldsymbol{b}(i)$. In other words, the trajectory optimization of the USV can enhance the accuracy of AUV state estimation.

4.2 Trajectory optimization of the USV

By controlling the motion of the USV, it is possible to achieve a desired USV–AUV configuration that optimizes the observability of the AUV in future steps. We define the USV state for future M steps as $\boldsymbol{X}_{\mathrm{s}}(i)=\left[\boldsymbol{x}_{\mathrm{s}}^{\mathrm{T}}(i|i),\boldsymbol{x}_{\mathrm{s}}^{\mathrm{T}}(i+1|i),\cdots,\boldsymbol{x}_{\mathrm{s}}^{\mathrm{T}}(i+M|i)\right]^{\mathrm{T}}$. Beginning with the current step i, the notation $(i+k|i)$ for $k=0,1,\cdots,M$ indicates the predicted k^{th} future step. The corresponding USV in-

Unedited

put sequence over the next M steps is denoted as $\boldsymbol{U}_{\mathrm{s}}(i) = \left[\boldsymbol{u}_{\mathrm{s}}^{\mathrm{T}}(i|i), \boldsymbol{u}_{\mathrm{s}}^{\mathrm{T}}(i+1|i), ..., \boldsymbol{u}_{\mathrm{s}}^{\mathrm{T}}(i+M|i)\right]^{\mathrm{T}}$.

Assuming that the AUV's velocity varies slowly over this future horizon, the cost function for the AUV observation at the future k^{th} step is defined as

$$F_1(k) = \sum_{a=1}^{3} \sqrt{\boldsymbol{b}(i+k|i)_a}. \tag{17}$$

To ensure the USV can effectively track the AUV, the tracking cost functions at the future k^{th} step are defined as

$$F_2(k) = d_1(i+k|i) + d_2(i+k|i), \tag{18}$$

$$F_3(k) = |\theta_{\mathrm{v}}(i+k|i)|, \tag{19}$$

where d_1 is the horizontal distance from the USV to the AUV, d_2 is the horizontal distance from the USV to the AUV's velocity direction, and θ_{v} is the angle between the velocity directions of the AUV and USV, as demonstrated in Fig. 4. These constraints pertain to the relative state of the USV with respect to the AUV and guide the USV to closely follow the AUV, thereby enhancing AUV observability over an extended time horizon.

We then obtain the total cost function:

$$F(k) = \alpha_1 F_1(k) + \alpha_2 F_2(k) + \alpha_3 F_3(k), \tag{20}$$

where α_1, α_2, and α_3 are the weighting parameters for each component of the cost function. The term $F_1(k)$ aims to enhance the AUV's observability by minimizing the uncertainty in its state prediction over a future horizon. However, if only $F_1(k)$ is considered, minimizing it may lead the USV to follow an optimization trajectory that moves away from the AUV. This occurs because, when the AUV and USV are in close proximity, increasing their separation maximizes the relative position difference, thereby reducing $F_1(k)$, as illustrated in section 3 of the supplementary materials. While this strategy improves observability in the short term, it compromises the USV's ability to maintain effective tracking of the AUV over an extended period, potentially leading to a loss of communication or observation.

To address this issue, $F_2(k)$ and $F_3(k)$ are introduced to impose constraints on the USV's tracking behavior. Specifically, $F_2(k)$ penalizes the horizontal distance between the USV and the AUV (d_1), and the distance between the USV and the AUV's velocity directions (d_2). The terms d_1 and d_2 ensure

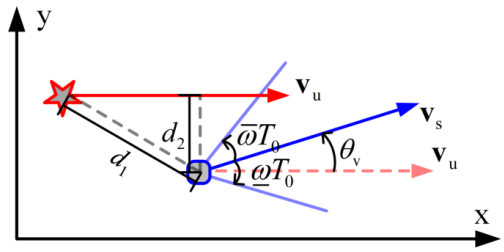

Fig. 4 Relationship between the velocity and position of AUV and USV

that the USV aligns with the motion trajectory of the AUV. Minimizing $F_2(k)$ keeps the USV in close proximity to the AUV, preventing the divergence caused by optimizing $F_1(k)$ alone, while ensuring the USV remains positioned for continuous observation of the AUV's motion.

Furthermore, minimizing $F_3(k)$ ensures that the USV adjusts its heading to align its velocity direction with that of the AUV, which is particularly important during sharp turns or dynamic maneuvers. Together, $F_2(k)$ and $F_3(k)$ balance the positional and angular constraints, enabling the USV to effectively track the AUV while preserving the AUV's observability over an extended time horizon.

To ensure the appropriate contribution of each component to the total cost function $F(k)$, the weighting parameters are set as $\alpha_1 = 1$, $\alpha_2 = 0.1$, and $\alpha_3 = 1$. The value of $\alpha_1 = 1$ prioritizes $F_1(k)$, emphasizing the importance of AUV observability, which is critical for accurate state estimation in navigation. However, since $F_2(k)$ typically involves distances on the order of meters (e.g., 1–10 m in the tested scenarios), its magnitude is significantly larger than that of $F_1(k)$ (0–1) and $F_3(k)$ (0–π radians). To balance its contribution, α_2 is set to 0.1, reducing the influence of $F_2(k)$, while still ensuring that the USV maintains proximity to the AUV, as illustrated in section 4 of the supplementary materials. The parameter $\alpha_3 = 1$ assigns equal importance to $F_3(k)$ as to $F_1(k)$, reflecting the critical role of angular alignment in dynamic tracking scenarios, such as the "SinFollow1" trajectory, where frequent turns require precise heading adjustments. This choice of weights ensures a balanced trade-off between observability and tracking performance, as validated through simulations in Section 5.

The following optimization problem is then solved in a receding horizon way to minimize the

Unedited

total cost function for the next M steps:

$$\boldsymbol{U}_{\mathrm{s}}^{*}(i)=\arg\min_{\boldsymbol{U}_{\mathrm{s}}(i)}\sum_{k=0}^{M}F(k), \tag{21}$$

s.t. for $k=0,1,\cdots,M$,

$$\begin{cases}\boldsymbol{x}_{\mathrm{u}}(i+k+1|i)=\boldsymbol{F}\boldsymbol{x}_{\mathrm{u}}(i+k|i),\ \boldsymbol{x}_{\mathrm{u}}(i|i)=\hat{\boldsymbol{x}}_{\mathrm{u}}(i),\\ \boldsymbol{x}_{\mathrm{s}}(i+k+1|i)=\boldsymbol{x}_{\mathrm{s}}(i+k|i)+\\ \begin{bmatrix} v_{\mathrm{s}}(i+k|i)\cos\psi_{\mathrm{s}}(i+k|i)\\ v_{\mathrm{s}}(i+k|i)\sin\psi_{\mathrm{s}}(i+k|i)\\ 0\\ \omega_{\mathrm{s}}(i+k|i)\end{bmatrix}T_0,\ \boldsymbol{x}_{\mathrm{s}}(i|i)=\boldsymbol{x}_{\mathrm{s}}(i),\\ \underline{\omega}\le\omega_{\mathrm{s}}(i+k|i)\le\bar{\omega},\\ \underline{v}\le v_{\mathrm{s}}(i+k|i)\le\bar{v},\end{cases} \tag{22}$$

where $\underline{\omega}$, $\bar{\omega}$, $\underline{v}$, and $\bar{v}$ represent the physical limits of the corresponding variables, with $\bar{v}=1.15\,\|[v_{\mathrm{u},x},v_{\mathrm{u},y}]\|$ and $\underline{v}=0.9\bar{v}$. Note that at the ith step, $\hat{\boldsymbol{x}}_{\mathrm{u}}(i)$ and $\boldsymbol{x}_{\mathrm{s}}(i)$ have been estimated and measured. Under the assumption of slowly varying velocity, the predicted AUV states over the next M steps can be obtained using $\hat{\boldsymbol{x}}_{\mathrm{u}}(i)$ as the initial state. Similarly, the predicted USV states over the next M steps depend on the USV control inputs $\boldsymbol{U}_{\mathrm{s}}(i)$ and are derived from the initial state $\boldsymbol{x}_{\mathrm{s}}(i)$. These predicted AUV and USV states determine the FIM matrix in Eq. (21), whose elements are defined as in Eq. (S6).

4.3 Solving the trajectory optimization problem

The problem defined by Eqs. (21)–(22) is highly nonlinear. Traditional local optimization methods, such as gradient descent, are ineffective for this problem, as they often converge to local optima or fail to converge due to the non-smooth nature of the cost function. To address this challenge without requiring explicit Jacobian computations, we employ the PSO technique. PSO begins with the initialization of a random solution and iteratively searches for the optimal solution. A group of moving particles forms a swarm, with the coordinates of each particle serving as the variables to be optimized. Based on the current best solution found by each individual particle and the global best solution found by the entire swarm, each particle continuously adjusts its speed and coordinates. The global optimal solution can be identified through iterations. The simulation results demonstrate that each optimization and localization step requires only 0.2 s, fully meeting the real-time processing requirements. In this study, we employ the linearly decreasing inertia weight PSO (LDIW-PSO) algorithm. By comparing the localization performance of various PSO variants, it is found that the varying PSO algorithms have a limited impact on the results. Therefore, we use LDIWPSO for solving the localization problem because of its simplicity and effectiveness. Algorithm 1 presents the corresponding pseudo-code to solve Eqs. (21) and (22) using PSO.

Algorithm 1 : Optimal motion control of USV at step $i+1$ $(i>N)$

Input: $\boldsymbol{x}_{\mathrm{u}}(i)$: AUV state estimation for the current step N; $[\boldsymbol{x}_{\mathrm{s}}(i-N+1|i),...,\boldsymbol{x}_{\mathrm{s}}(i|i)]^{\mathrm{T}}$: N historical states of USVs

Output: optimal USV state at $(i+1)^{\mathrm{th}}$ step $\boldsymbol{u}_{\mathrm{s}}(i+1|i)=[v_{\mathrm{s}}(i+1|i),\omega_{\mathrm{s}}(i+1|i)]^{\mathrm{T}}$

```
Randomly initialized particle swarm
Set the maximum number P of iterations
Set the iteration number p = 1
Set the number of predicted steps M
Initialize particle coordinates
while p ⩽ P do
    Update particle coordinates that satisfy the constraint boundaries
    Evaluate the cost function value of the particle F(u_s(i+1|i), ..., u_s(i+M|i))
    Update the historical optimal position and the global optimal position of the particle
    p = p + 1
end while
Return: u_s^*(i+1|i)
```

To improve AUV observability in the next step, the desired USV–AUV geometry can be obtained by applying the optimal control input $\boldsymbol{u}_{\mathrm{s}}^{*}(1|i)$ to the USV.

The AUV can be tracked using a rolling horizon method by continuously estimating its state, as shown in Section 3. Here, the trajectory optimization of the USV can be used to optimize the measurement configuration and, consequently, the estimation accuracy. The closed-loop FOA-based USV–AUV navigation is accomplished by iteratively repeating these steps, as illustrated in Fig. 5.

5 Simulations and discussions

This section conducts simulations to demonstrate the effectiveness of the proposed estimation and trajectory optimization algorithms. Furthermore, we investigate the impact of variables on the

Unedited

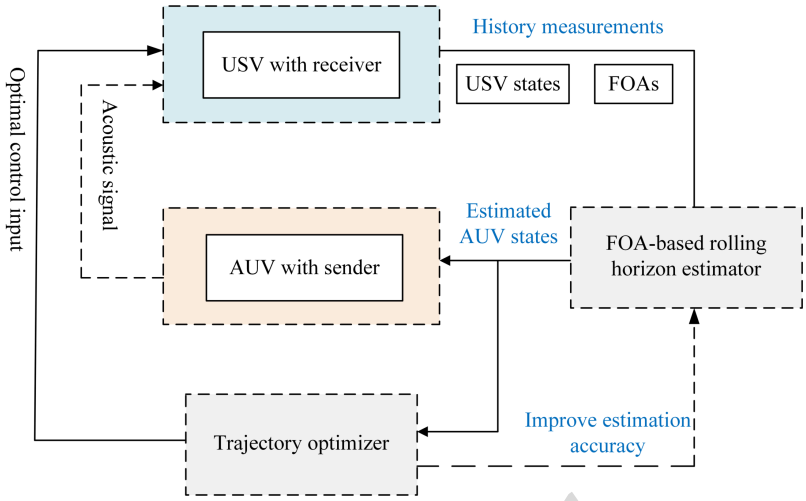

Fig. 5 Closed-loop FOA-based USV–AUV navigation

Unedited

USV–AUV navigation performance, including the USV trajectory, the complexity of the AUV trajectory, the AUV depth, measurement frequency, packet loss rate, and noise levels.

5.1 Optimized USV trajectory

The description of the simulation environment and simulation settings is provided in section 5 of the supplementary materials. The USV trajectory affects the frequency signal measurement geometry, which in turn impacts observability and estimation accuracy of the AUV. To demonstrate the superior estimation performance with the optimized USV trajectory, we compare six types of USV trajectories: the optimized trajectory, a straight-line trajectory, the "LinearFollow" trajectory, and three "SinFollow" trajectories. In multi-measurement steps, a large FIM will yield a small CRLB when the relative position and velocity differences between the AUV and USV are large, leading to substantial Doppler shift difference. In contrast, when the USV moves along a straight line, the relative state between the AUV and USV provides poor observability, as the relative position and velocity differences between the AUV and USV are small, as illustrated in section 3 of the supplementary materials. From a theoretical perspective, the optimized trajectory, derived by minimizing the cost function $F(k)$, balances AUV observability ($F_1(k)$) and USV tracking performance ($F_2(k)$ and $F_3(k)$). The term $F_1(k)$ enhances observability by maximizing relative state differences, thereby improving the FIM. However, solely minimizing $F_1(k)$ may drive the USV away from the AUV, increasing the tracking distance, as discussed in Section 4. The terms $F_2(k)$ and $F_3(k)$ mitigate this by penalizing the distance (d_1, d_2) and velocity angular deviation (θ_v) between the AUV and USV, ensuring proximity and alignment with the AUV's motion. This balance is critical in dynamic scenarios (e.g., "SinFollow" trajectories), where frequent AUV turns require rapid USV adjustments.

Figs. S6–S8 in the supplementary materials illustrate the USV moving along the optimized trajectory, and the four specific trajectories of USV above the AUV in Cases 1, 3, and 5, respectively. Simulation results validate these theoretical insights. All five USVs can track and estimate the AUV to varying degrees using the proposed FOA-based estimation method. However, as the AUV's turning rate increases, the USV's tracking and estimation accuracy deteriorates. Notably, the optimized USV consistently achieves the best tracking performance, as $F_1(k)$ guarantees observability, while $F_2(k)$ and $F_3(k)$ enable the USV to track the AUV. Note that we conducted simulations in Case 1 with the state noise of the AUV and USV follows different heavy-tailed distributions. Results show that the estimation errors under heavy-tailed distributions are larger than those under the Gaussian distribution. These findings confirm that the deviation from the Gaussian noise assumption would increase estimation errors.

Moreover, the USV control inputs are shown in Figs. S9 and S10. All control inputs are contained

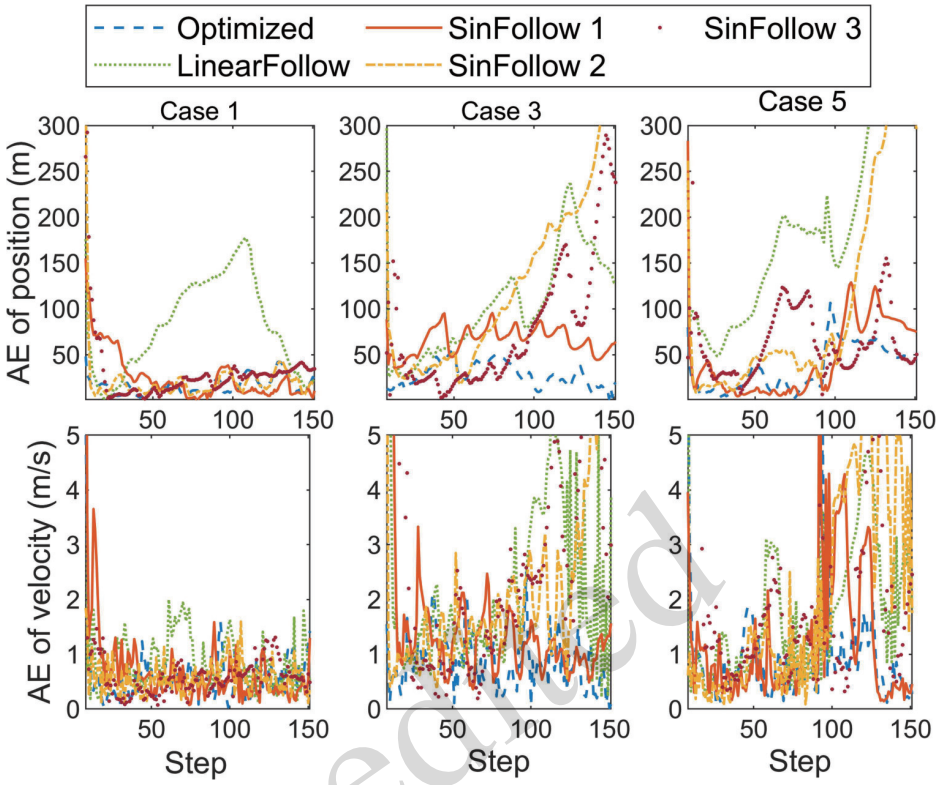

Fig. 6 AE of the estimated position and velocity

Unedited

within the physical limits of the system. The mean absolute speed (MAS) and mean absolute turning rate (MATR) reflect the USV's energy consumption:

$$\mathrm{MAS} = \frac{1}{E}\sum_{e=1}^{E}\frac{1}{I}\sum_{i=1}^{I}|v_{\mathrm{s}}(i,e)|, \tag{23}$$

$$\mathrm{MATR} = \frac{1}{E}\sum_{e=1}^{E}\frac{1}{I}\sum_{i=1}^{I}|\omega_{\mathrm{s}}(i,e)|. \tag{24}$$

The optimized USV trajectory does not have the highest cost in either speed or turning rate, with a minimum speed of 2.18 m/s in Case 5. Meanwhile, the "LinearFollow" trajectory incurs the lowest energy cost in terms of turning rate, with a minimum of 0.03 rad/s in Case 1.

Fig. 6 shows the absolute errors (AE) of the estimated position and velocity. The optimized USV trajectory is designed to enhance the USV–AUV geometry, thereby improving AUV observability and achieving the highest estimation accuracy. In contrast, the "LinearFollow" trajectory yields the poorest estimation accuracy, despite having the lowest energy consumption in terms of turning rate. The three "SinFollow" trajectories exhibit varying levels of estimation accuracy across different cases.

Additionally, Monte Carlo experiments are conducted. Fig. 7 shows the MAS and MATR of the USV control inputs. The optimized USV trajectory achieves the lowest MAS in all five cases, consistently below 2.19 m/s, while the MAS of other USV trajectories exceeds 2.19 m/s, with the "LinearFollow" trajectory in Case 4 reaching the highest value of 2.2634 m/s. The "LinearFollow" trajectory has the lowest MATR, followed by "SinFollow 3". The three highest MATRs are observed in "SinFollow 2", the optimized trajectory, and "SinFollow 1", all approximately 0.08 rad/s.

Fig. 8 presents the root mean square error (RMSE) of the estimated position and velocity. The "LinearFollow" trajectory exhibits the largest RMSE for position estimation, while "SinFollow 3" has the highest RMSE for velocity estimation in most cases. The optimized USV has the lowest RMSE for position and velocity estimation, with RMSEs for position that are 1.58–10.6 times lower and for velocity that are 1.34–12.6 times lower than those of the other trajectories. Except for the "LinearFollow" tra-

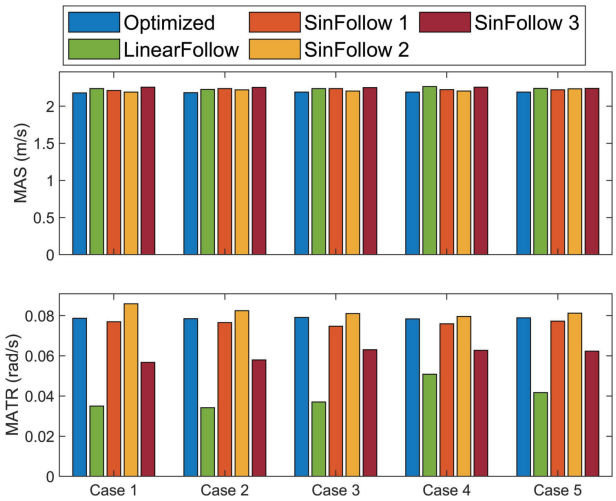

Fig. 7 MAS and MATR of the USV control inputs

jectory, all other USV trajectories achieve their lowest position RMSE in Case 1. The highest position RMSE values for all USV trajectories occur in Case 4, where the AUV has the largest turning rate. The highest velocity RMSE appears in Cases 2 and 4, while the lowest occurs in Cases 1 and 3.

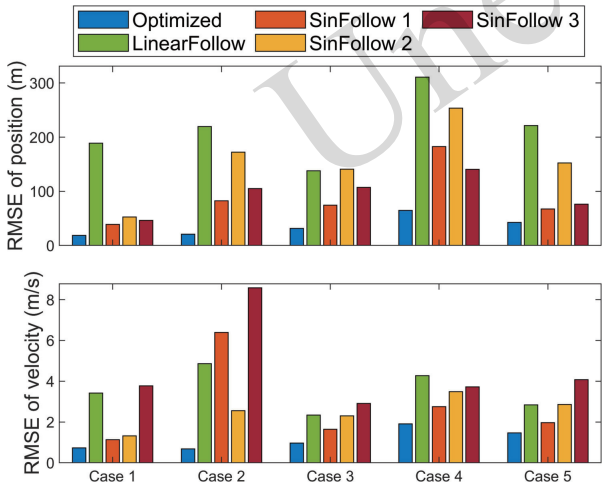

Fig. 8 RMSE of estimated position and velocity. Line: the "LinearFollow" trajectory; Sin1, Sin2, and Sin3: the three "SinFollow" trajectories

5.2 Impact of different factors

With the proposed FOA-based state estimation method, besides the USV trajectory, the observability of the AUV is influenced by various factors, including the AUV depth, the estimation horizon N, the packet loss rate of AUV depth P_l, the USV acceleration noise, and the time interval between steps T_0. Fig. 9 shows the MAS and MATR of the USV control inputs for speed and turning rate across different factors, while Fig. 10 shows the RMSE of AUV state estimation. Keep in mind that the distance between the AUV and USV affects the distance-dependent measurement noise. It is evident that in all cases, the USV with optimized trajectories can reliably estimate the AUV state. We then provide general instructions for using the proposed estimation algorithm and conduct a more thorough analysis of how various factors affect the performance of the FOA-based estimation.

5.2.1 Varying AUV depths

Theoretically, AUV depth affects the observability through the FOA measurement model. The FOA measurement, given by Eq. (9), depends on the relative geometry between the AUV and USV. As the AUV depth increases, the relative position difference between the AUV and USV decreases; in most cases, the relative velocity also reduces as the radial velocities $v_{\mathrm{u},\perp}(i)$ and $v_{\mathrm{s},\perp}(i)$ decrease, resulting in a reduced Doppler shift. Consequently, the observability (quantified by $F_1(k)$) diminishes as the relative state between the AUV and USV diminishes. Moreover, greater depths increase the propagation distance l, amplifying the distance-dependent noise in Eq. (12), further degrading estimation accuracy.

Fig. 9 illustrates the energy consumption in terms of USV speed and turning rate, while Fig. 10 depicts the RMSE at five different AUV starting depths, ranging from 0 m to 200 m. Overall, shallower AUV depths require higher USV speeds but lower turning rates. In Cases 1 and 2, where the AUV has a low turning rate, the AUV starting at a depth of 0 m yields the smallest RMSE: approximately 14 m for the position RMSE and 0.6 m/s for the velocity RMSE. In contrast, the AUV starting at 200 m results in the largest RMSE, with a position RMSE of about 25 m and a velocity RMSE of 0.9 m/s, demonstrating that shallower depths significantly enhance AUV observability and lead to improved estimation performance. The RMSE shows weaker correlation with AUV depth in Cases 3–5, where the AUV has a larger turning rate. Notably, in Cases 3 and 4, the largest RMSE occurs at a depth of 0 m, with the position RMSEs of 89.5 m and 172.4 m and the velocity RMSEs of 1.51 m/s and 2.56 m/s. This evidence suggests that for straighter AUV trajectories with lower turning rates, shallower depths result

Unedited

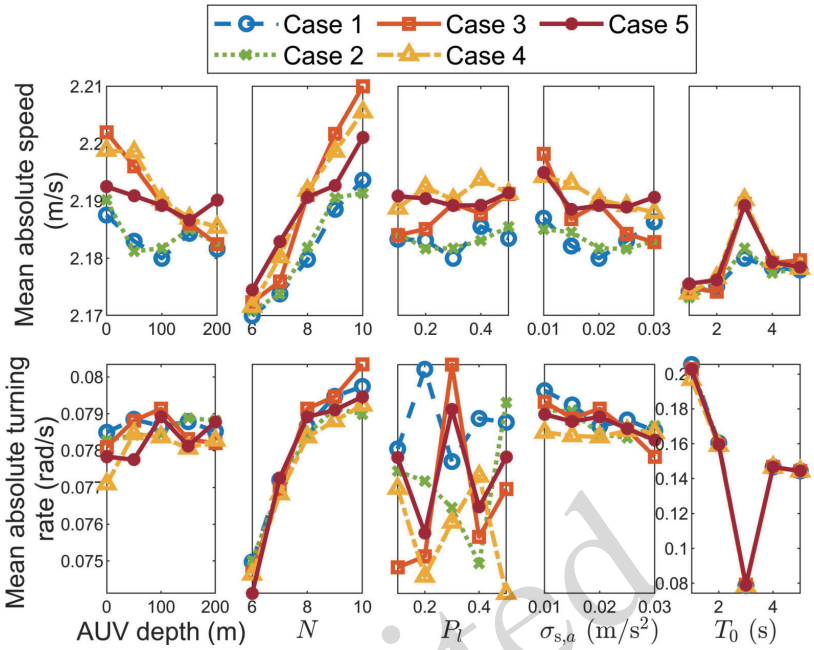

Fig. 9 MAS and MATR of the USV control inputs across different factors

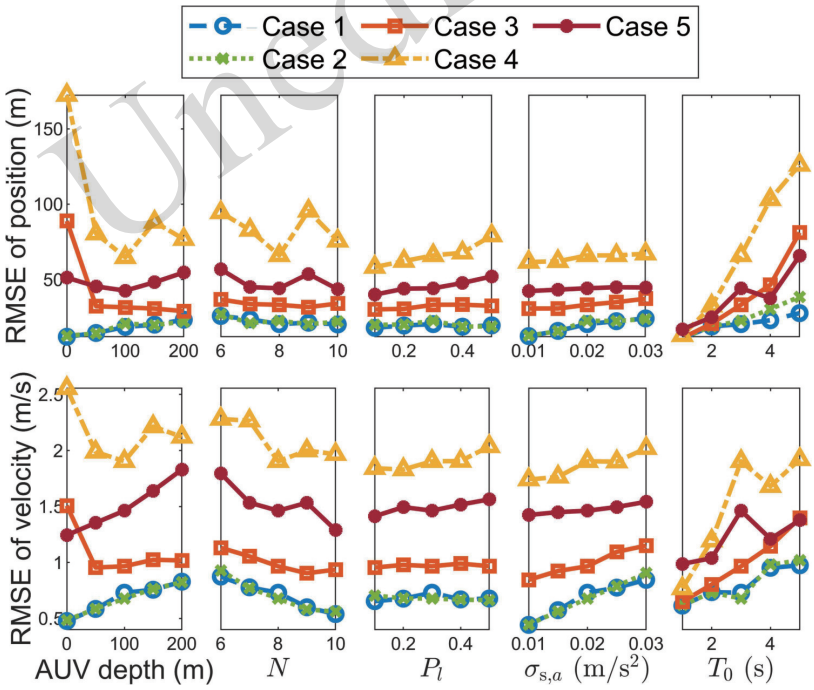

Fig. 10 RMSE of AUV state estimation across different factors

Unedited

in better AUV observability. For shallower AUV depths, the relative state change between the AUV and USV is greater, providing additional information in the measurements and resulting in improved observability. However, when the AUV turning rate is high, the assumption of constant AUV velocity over N steps becomes less valid, leading to larger errors as the relative state increases. By comparing the results in Figs. 9 and 10, we conclude that improved AUV observability is achieved at the cost of increased energy consumption.

5.2.2 Varying estimation horizons N

The estimation horizon N plays an important role in determining the estimation results, as it governs the amount of information used in the state estimation process. Theoretically, an increased N includes additional FOA measurements, improving observability, and reducing estimation uncertainty. However, in dynamic scenarios with high AUV turning rates, an excessively large N may include outdated measurements, leading to errors due to the AUV's rapid state changes.

Figs. 9 and 10 illustrate the effect of varying N from 6 to 10. As N increases, the USV incorporates more measurement data into the estimation process, resulting in generally lower RMSEs. For instance, in Case 1, increasing N from 6 to 10 reduces the position RMSE from 24.0 m to 18.3 m, and the velocity RMSE decreases from 0.87 m/s to 0.54 m/s, as more measurements improve the estimation accuracy, consistent with the theoretical prediction. In scenarios with elevated AUV turning rates (e.g., Case 4), the benefit of a larger N is diminished due to the swiftly fluctuating AUV dynamics, resulting in a position RMSE consistently near 80 m irrespective of N. This evidence indicates that, although an extended estimation horizon enhances accuracy for linear AUV trajectories, its efficacy diminishes when tracking high-turning-rate trajectories. Energy consumption is impacted: as N increases, the MAS and MATR of the USV slightly rise to maintain the increased demand for accurate tracking. In Case 1, for example, the MAS shifts from 2.17 m/s at $N = 6$ to 2.19 m/s at $N = 10$, indicating a minor increase in energy usage due to extended observation time.

5.2.3 Varying packet loss rate P_l

The packet loss rate P_l affects the availability of FOA measurements for state estimation. Theoretically, a higher P_l reduces the number of effective measurements, thereby decreasing observability and increasing estimation error. The FOA measurement model assumes that each measurement contributes to the state update; with packet loss, the update frequency decreases, leading to larger errors in the Kalman filter's prediction step.

When trajectories are more straight, such as those in Cases 1–3, P_l has almost no effect on RMSE. This means that the USV can keep accurate tracking even under high packet loss rate. In these cases, the position RMSEs stabilize around 17.3 m, 17.5 m, and 30.3 m, while the velocity RMSEs are approximately 0.68 m/s, 0.68 m/s, and 0.98 m/s, respectively. These results demonstrate that simpler trajectories yield smaller RMSEs and highlight the resilience of the estimation process in less dynamic scenarios. In contrast, for more complex trajectories (e.g., Cases 4 and 5), P_l has a significantly greater effect. For instance, in Case 4, increasing P_l from 0.01 to 0.03 raises the position RMSE from 56.8 m to 78.0 m and the velocity RMSE from 1.84 m/s to 2.04 m/s. These higher RMSEs reflect the challenge of tracking dynamic trajectories when depth data is frequently lost. The effect of P_l on energy consumption is less consistent across different cases. Generally, to compensate for increased packet loss, the USV expends more energy by adjusting its control inputs.

5.2.4 Varying USV acceleration noise $\sigma^2_{\mathrm{s,a}}$

The USV acceleration noise $\sigma^2_{\mathrm{s,a}}$ introduces variability into the USV's motion, hence impacting the precision of FOA measurements. The variance $\sigma^2_{\mathrm{s,a}}$ varies with sea state and depth (Holthuijsen, 2010): the rougher the sea and the shallower the USV depth, the higher the $\sigma^2_{\mathrm{s,a}}$. In theory, a higher $\sigma^2_{\mathrm{s,a}}$ increases the uncertainty in the USV's position and velocity, which propagates to the FOA measurement, as the USV's position and velocity affect the Doppler shift. This increased uncertainty reduces observability and degrades estimation accuracy.

Increased $\sigma^2_{\mathrm{s,a}}$ introduces variability into the USV's movements, affecting both RMSE and energy consumption. As $\sigma^2_{\mathrm{s,a}}$ rises, the USV's control accuracy declines, leading to larger RMSEs. For instance, in Case 1, increasing $\sigma^2_{\mathrm{s,a}}$ from 0.01 m/s^2 to 0.03 m/s^2 raises the position RMSE from 10.4 m to 22.3 m and the velocity RMSE from 0.44 m/s to 0.85 m/s, consistent with the theoretical prediction. In Case 4, the position RMSE can reach up to 60 m with a higher $\sigma^2_{\mathrm{s,a}}$. Additionally, with lower $\sigma^2_{\mathrm{s,a}}$, the USV increases its speed and turning rate, resulting in higher energy consumption.

5.2.5 Varying time interval between Steps T_0

The time interval T_0 between measurement steps impacts estimation accuracy and energy consumption. Theoretically, a larger T_0 reduces the

Unedited

update frequency, increasing the prediction error in the Kalman filter, as the AUV state may change substantially between updates. This effect is more pronounced in dynamic scenarios, where the AUV's velocity and direction change rapidly.

Larger T_0 values reduce update frequency, leading to higher RMSE. For instance, in Case 2, increasing T_0 from 1 s to 5 s raises the position RMSE from 9.3 m to 36.8 m and the velocity RMSE from 0.62 m/s to 1.02 m/s, confirming the theoretical prediction. In more complex scenarios, such as Case 4, the position RMSE exceeds 125.4 m with a 5 s interval, highlighting the need for frequent updates to maintain tracking accuracy under dynamic conditions. Additionally, as T_0 increases, energy consumption for speed control generally rises, while that for turning rate generally decreases, reflecting the adjustments required by the USV. Notably, at $T_0 = 3$ s, speed and turning rate deviate from the overall trend, although the general pattern remains consistent.

In summary, the performance of the USV–AUV navigation system is influenced by multiple factors. For AUV trajectories, greater curvature (i.e., fewer straight paths) leads to lower estimation accuracy and increased energy consumption, as the USV must make more frequent and intensive adjustments to follow the AUV accurately. Higher noise levels, particularly in the USV acceleration, result in reduced tracking precision, which negatively affects RMSE and energy consumption. Conversely, higher measurement frequency, lower packet loss rates, and a larger estimation horizon (i.e., more information) improve estimation accuracy, as the USV has more data to rely on, especially when tracking complex trajectories. Finally, scenarios with less dynamic variation, where AUV velocity and direction change more gradually, allow for improved tracking accuracy and reduced energy consumption, as the USV can follow the AUV's trajectory more predictably. Overall, smoother trajectories, lower noise, more frequent updates, and reduced dynamic changes contribute to optimal performance in terms of accuracy and efficiency.

6 Conclusions

This paper considers using only a single surface sensor node (USV) to estimate the states of a moving underwater target (AUV), i.e., the navigation problem. Particular attention is paid to achieving the optimal geometry for measuring the FOA signals to maximize system observability and thus improve the estimation accuracy in complex underwater environments. These goals are achieved by proposing FOA-based state estimation and USV trajectory optimization algorithms, with a tailored cost function that integrates the CRLB to optimize observability, a distance component to ensure close following, and a turning rate component to maintain alignment. The proposed FOA-based framework enables robust AUV state estimation without requiring time synchronization between AUV and USV.

From this work, we conclude that, in many cases, a randomly generated trajectory for a single surface node may fail to estimate the AUV state. The proposed CRLB-based trajectory optimization algorithm provides a degree of guaranteed state estimation performance. The effectiveness of this algorithm is supported by a theoretical analysis of the FOA measurement model, which quantifies the impact of observability on estimation accuracy. Several factors are shown to significantly influence the accuracy of FOA-based estimation: the complexity of the AUV trajectory, noise levels, measurement frequency, and packet loss rate. Specifically, straighter AUV trajectories yield higher estimation accuracy and lower energy consumption for the USV. Lower noise levels, higher measurement frequency, and reduced packet loss rates further improve tracking accuracy and efficiency. Additionally, shallower AUV depths and larger estimation horizons enhance system observability, making it generally favorable when using the proposed algorithm.

Contributors

Wen XU conceptualized the study, acquired the funding, and administrated the project. Huarong ZHENG and Wen XU supervised the research. Sitian WANG proposed the methodology, developed the software, performed the visualization, and drafted the paper. Huarong ZHENG and Jianlong LI validated the results. Huarong ZHENG and Wen XU reviewed and edited the final paper.

Conflict of interest

All the authors declare that they have no conflict of interest.

Data availability

Unedited

The data that support the findings of this study are available from the corresponding author upon reasonable request.

References

Becker C, Ribas D, Ridao P, 2012. Simultaneous sonar beacon localization & AUV navigation. *IFAC Proc Vol*, 45(27):200-205. https://doi.org/10.3182/20120919-3-IT-2046.00034

Cameron KJ, 2018. FDOA-based passive source localization: a geometric perspective. PhD Dissemination, Colorado State University, Fort Collins, USA.

Chen HF, Xie L, Shen CQ, 2015. Optimal Byzantine attack strategy for distributed localisation with M-ary quantised data. *Electron Lett*, 51(25):2158-2160. https://doi.org/10.1049/el.2015.2172

Conti A, Mazuelas S, Bartoletti S, et al., 2019. Soft information for localization-of-things. *Proc IEEE*, 107(11):2240-2264. https://doi.org/10.1109/JPROC.2019.2905854

De Palma D, Arrichiello F, Parlangeli G, et al., 2017. Underwater localization using single beacon measurements: observability analysis for a double integrator system. *Ocean Eng*, 142:650-665. https://doi.org/10.1016/j.oceaneng.2017.07.025

Fallon MF, Papadopoulos G, Leonard JJ, et al., 2010. Cooperative AUV navigation using a single maneuvering surface craft. *Int J Robot Res*, 29(12):1461-1474. https://doi.org/10.1177/0278364910380760

Fossen TI, 2011. Handbook of marine craft hydrodynamics and motion control. John Wiley & Sons, Chichester, UK.

Gong ZJ, Li C, Su RY, 2023. Fundamental limits of Doppler shift-based, ToA-based, and TDoA-based underwater localization. *IEEE/CAA J Autom Sin*, 10(7):1637-1639. https://doi.org/10.1109/JAS.2023.123282

Guo HR, Qian ZW, Wang XJ, et al., 2023. A robust attitude estimation algorithm for seabed inverted ultra-short baseline. *Ocean Eng*, 280:114534. https://doi.org/10.1016/j.oceaneng.2023.114534

Han YF, Shi CH, Sun DJ, et al., 2018. Research on integrated navigation algorithm based on ranging information of single beacon. *Appl Acoust*, 131:203-209. https://doi.org/10.1016/j.apacoust.2017.10.029

Holthuijsen LH, 2010. Waves in oceanic and coastal waters. Cambridge university press, Cambridge, USA.

Jiang C, Li JL, Xu W, et al., 2021. Improvement of the position estimation for underwater gliders with a passive acoustic method. *IEEE J Oceanic Eng*, 46(4):1165-1178. https://doi.org/10.1109/JOE.2021.3085096

Kim J, 2023. Underwater transmitter localization based on TDOA and FDOA considering the unknown time-varying emission frequency. *J Mar Sci Eng*, 11(7):1260. https://doi.org/10.3390/jmse11071260

Kinsler LE, Frey AR, Coppens AB, et al., 2000. Fundamentals of Acoustics. 4th ed. John Wiley & Sons, Hoboken, USA.

Lee PM, Jun BH, 2007. Pseudo long base line navigation algorithm for underwater vehicles with inertial sensors and two acoustic range measurements. *Ocean Eng*, 34(3-4):416-425. https://doi.org//10.1016/j.oceaneng.2006.03.011

Moreno-Salinas D, Pascoal A, Aranda J, 2016. Optimal sensor placement for acoustic underwater target positioning with range-only measurements. *IEEE J Oceanic Eng*, 41(3):620-643. https://doi.org/10.1109/JOE.2015.2494918

Nguyen NH, Dogancay K, 2018. Closed-form algebraic solutions for 3-D Doppler-only source localization. *IEEE Trans Wirel Commun*, 17(10):6822-6836. https://doi.org/10.1109/TWC.2018.2864680

Ostachowicz W, Soman R, Malinowski P, 2019. Optimization of sensor placement for structural health monitoring: A review. *Struct Health Monit*, 18(3):963-988. https://doi.org/10.1177/1475921719825601

Qu JQ, Li XG, Sun GW, 2021. Optimal formation configuration analysis for cooperative localization system of multi-AUV. *IEEE Access*, 9:90702-90714. https://doi.org/10.1109/ACCESS.2021.3090514

Ramezani H, Jamali-Rad H, Leus G, 2013. Target localization and tracking for an isogradient sound speed profile. *IEEE Trans Signal Process*, 61(6):1434-1446. https://doi.org/10.1109/TSP.2012.2235432

Rypkema NR, 2019. Underwater & out of sight : towards ubiquity in underwater robotics. Massachusetts Institute of Technology, Cambridge, USA.

Sahu N, Wu LL, Babu P, et al., 2022. Optimal sensor placement for source localization: a unified ADMM approach. *IEEE Trans Veh Technol*, 71(4):4359-4372. https://doi.org/10.1109/TVT.2022.3146603

Stojanovic M, Preisig J, 2009. Underwater acoustic communication channels: propagation models and statistical characterization. *IEEE Commun Mag*, 47(1):84-89. https://doi.org/10.1109/MCOM.2009.4752682

Tan YT, Gao R, Chitre M, 2014. Cooperative path planning for range-only localization using a single moving beacon. *IEEE J Oceanic Eng*, 39(2):371-385.

Wang ST, Zheng HR, Zhang T, et al., 2025. Frequency and time of arrival based moving target state estimation with underwater distributed sensor network. *Ocean Eng*, 334:121563. https://doi.org/10.1016/j.oceaneng.2025.121563

Webster SE, Eustice RM, Singh H, et al., 2012. Advances in single-beacon one-way-travel-time acoustic navigation for underwater vehicles. *Int J Robot Res*, 31(8):935-950. https://doi.org/10.1177/0278364912446166

Win MZ, Shen Y, Wymeersch H, 2008. On the position error bound in cooperative networks: a geometric approach. Proc 10th Int Symp Spread Spectrum Techniques and Applications, Bologna, Italy, p.637-643. https://doi.org/10.1109/ISSSTA.2008.125

Xu B, Fei YL, Wang XY, et al., 2023. Optimal topology design of multi-target AUVs for 3D cooperative localization formation based on angle of arrival measurement. *Ocean Eng*, 271:113758. https://doi.org/10.1016/j.oceaneng.2023.113758

Yu Y, Zheng HR, Xu W, 2025. Learning and sampling-based informative path planning for AUVs in ocean current fields. *IEEE Trans Syst Man Cybern Syst*, 55(1):51 - 62. https://doi.org/10.1109/TSMC.2024.3370177

Zhan DZ, Wang ST, Cai SG, et al., 2023. Acoustic localization with multi-layer isogradient sound speed profile using TDOA and FDOA. *Front Inform Technol Electron Eng*, 24(1):164-175. https://doi.org/10.1631/FITEE.2100398

Unedited

Zhang BB, Ji DX, Liu S, et al., 2023. Autonomous underwater vehicle navigation: a review. *Ocean Eng*, 273:113861.
https://doi.org/10.1016/j.oceaneng.2023.113861

Zhang DQ, Ashraf MA, Liu ZL, et al., 2020. Dynamic modeling and adaptive controlling in GPS-intelligent buoy (GIB) systems based on neural-fuzzy networks. *Ad Hoc Netw*, 103:102149.
https://doi.org/10.1016/j.adhoc.2020.102149

Zheng HR, Liu CG, 2025. An overview of unmanned surface vehicles: methods, practices, and applications. *Control Eng Pract*, 164:106479.
https://doi.org/10.1016/j.conengprac.2025.106479

Zheng HR, Li JC, Tian ZE, et al., 2024. Hybrid physics-learning model based predictive control for trajectory tracking of unmanned surface vehicles. *IEEE Trans Intell Transport Syst*, 25(9):11522-11533.
https://doi.org/10.1109/TITS.2024.3374796

Zhu ZB, Hu SLJ, 2018. Model and algorithm improvement on single beacon underwater tracking. *IEEE J Oceanic Eng*, 43(4):1143-1160.
https://doi.org/10.1109/JOE.2017.2754018

List of supplementary materials

1 Sequential EKF process
2 Fisher information matrix for AUV state estimation
3 Optimal USV trajectory planning for AUV state estimation
4 Parameter selection and sensitivity analysis for the cost function
5 Simulation parameters and experimental setup
6 Comparative analysis of USV trajectory performance
Table S1 Parameter sensitivity analysis in Case 1
Table S2 Default parameters for the USV–AUV navigation
Table S3 Default noise standard deviations
Table S4 Initial USV state settings for the simulation
Figs. S1–S4 Relationship between the USV's velocity direction (relative to the x-axis) and the sum of the FIM diagonal elements under varying relative positions
Fig. S5 AUV trajectories in Case 1–5
Fig. S6 Four USV specific trajectories labeled for the true AUV trajectory in Case 3
Fig. S7 USV moves along the optimized trajectory and the four specific trajectories in Case 1
Fig. S8 USV moves along the optimized trajectory and the four specific trajectories in Case 3
Fig. S9 USV moves along the optimized trajectory and the four specific trajectories in Case 5
Fig. S10 USV speed control inputs
Fig. S11 USV turning rate control inputs

Unedited